Single-molecule detection of chaperonin dynamics through polarization rotation modulation of CdSe QD luminescence imaging

Single-molecule Detection of Chaperonin Dynamics through Polarization Rotation Modulation of CdSe QD Luminescence Imaging

Toshiro Tani[1,*], Masaru Oda[1,**], Daisuke Araki[2], Tatsuki Miyashita[2], Koudai Nakajima[2], Mayuno Arita[3], Masafumi Yohda[4]

[1]Division of Advanced Applied Physics, [2]Department of Applied Physics, [3]Department of Biotechnology and Life Science, [4]Division of Biotechnology and Life Science, Tokyo University of Agriculture and Technology, Institute of Technology, Naka-cho 2-24-16, Kogane-i, Tokyo 184-8588, Japan

* Corresponding author: (T. Tani) Tel: +81-42-388-7153, Fax: +81-42-385-6255, E-mail: ttani@cc.tuat.ac.jp,

** Present address: Department of Basic Sciences, Faculty of Engineering, Kyushu Institute of Technology, 1-1 Sensui-cho, Tobata-ku, Kitakyushu, Fukuoka 804-8550, Japan

Abstract: We report our recent trials examining the single-molecule three-dimensional (3D) detection of protein conformational dynamics at room temperature. Using molecular chaperones as model proteins and cadmium selenide (CdSe) semiconductor quantum dots (QDs) as nanometer-scale probes, we monitored the temporal evolution of ATP-induced conformation changes with a total internal reflection fluorescence (TIRF) microscopy imaging technique in buffer solutions. The two-dimensional (2D) degenerate nature of the emission dipoles of the QDs, due to the uniaxial wurtzite crystal structure, made it possible to capture the 3D orientation using a polarization modulation technique in real time. The temporal resolution was half the period of analyzer rotation. Although still insufficient, the obtained signals suggest possible 3D detection of specific motions, which supports the two-step conformational changes triggered by ATP attachment.

PACS codes: 81.05.-t; 81.07.-b; 81.16-c; 81.20.-n; 82.37.-j
Keywords: single-molecule imaging, protein dynamics, polarization modulation, CdSe/ZnS quantum dot (QD), molecular chaperone, chaperonin (CPN)

Main text:

1. Introduction

Cadmium selenide (CdSe) semiconductor nanocrystals prepared using the colloidal method have attracted attention as quantum dots (QDs) due to their high photoluminescence quantum yield with high optical stability, and organic ligand surfactant nature on their outermost surfaces [1]. They are distinguished not only by the quantum confinement of their electronic structures, but also by their high biochemical affinities. Our current research interest is in their possible use as molecular probes for determining the three-dimensional (3D) orientation of single molecules, such as in protein dynamics [2].

This possibility arises from the intrinsic electronic nature of QDs, which usually have uniaxial wurtzite crystal structures [3]. This crystallographic feature results in twofold degenerate emission dipoles within the *a*,*b*-plane, perpendicular to the *c*-axis, at room temperature [4, 5]. This twofold degeneracy appears as a circularly symmetric distribution of linearly polarized emissions.

As we observe the projection of the emission dipole on the sample surface, *i.e.*, the two-dimensional (2D) detector imaging surface, in single-molecule microscopy, the detected distribution becomes elliptical according to the tilt angle of the *c*-axis. The maximum and minimum components of the emission dipole distribution, or its ellipticity, can be monitored simply by inserting and rotating a linear analyzer. In this technique, it is essential for this ellipticity to be determined as is, without any further references. Then, the temporal resolution becomes half of the rotation period. The 3D orientation of the *c*-axis of the QD can eventually be obtained if its longitude is determined. The initial phase of the modulation signal brought about by the rotating analyzer is a good measure of its relative longitude. Consequently, by attaching such QDs to a protein as nanoprobes, we can trace the protein dynamics both spatially and temporally [6].

As model proteins, we have been studying the molecular chaperones prefoldin (PFD) and chaperonin (CPN) [6 – 10]. Both are Group II chaperonins and are present in eukaryotes and Archaea (*i.e.*, thermosomes). They both possess large central cavities that capture denatured polypeptides and are responsible for biochemical functions, such as transfer and refolding. Compared with Group I chaperonins, such as GroEL, they lack a GroES-like cap, but have a built-in lid that enables them to encapsulate unfolded proteins. Here, we consider CPNs specifically. These molecules consist of double back-to-back octameric-ring assemblies of ca. 60-kDa subunits. This is important to understand the relationships among ATP binding, hydrolysis events, and the lid-closure folding motions [11, 12]. Direct observations at the single-molecule level, although essentially stochastic, are needed.

2. Experiments

Figure 1 shows the sample preparation scheme. Chaperonins (CPNs) from the hyperthermophilic archaeon *Thermococcus* KS1 were used [11]. Briefly, the CPNs used were

mutants in which Asp-263 and Cys-366 of the wild-type CPNs had been replaced by Cys and Ser, respectively. The former makes it possible to connect QDs at the top end of the helical protrusions (HPs) in the apical domain through a linker via the maleimide-thiol coupling reaction. HPs from eight subunits form the built-in lid mentioned above. Cys-366 in the intermediate domains is replaced to prevent other QDs from coupling here and to secure the built-in lid. We used *N*-succinimidyl-4-(*N*-maleimidomethyl) cyclohexane-1-carboxylate (SMCC) as a linker. As CPNs are transparent and not luminescent in the visible region ($\lambda_{ab}^{(p)}$ ~280 nm), we connected the organic fluorescent probe, Cy5s ($\lambda_{ab}^{(p)}$ = 649 nm, $\lambda_{em}^{(p)}$ = 670 nm), to allow traceability during microscope imaging.

As the CdSe QDs, we used Qdot® 565 nanocrystals (Invitrogen; $\lambda_{ab}^{(p)}$ = 543 nm, $\lambda_{em}^{(p)}$ = 565 nm). The structure is also shown in Fig. 1. As shown in the figure, the QDs are ca. 15 nm in diameter, making them almost as large as the CPNs, and there are several tens of amino groups externally available for connecting the linker. This was an advantage for our preliminary trials.

These components are coupled to each other sequentially, under precise, careful control of the reaction conditions and separation and purification protocols in specific buffer solutions. Further details of the respective protocols and related reagents are described elsewhere.

We performed single-molecule microscopy with a total internal reflection fluorescence (TIRF) configuration. Briefly, the main optics were modified from a versatile inverted optical microscope (TE-2000U; Nikon) with numerical aperture (N.A.) = 1.45 oil-immersion objective (×100). Two lasers (532 and 633 nm) served as excitation sources with typical intensities of $45 - 60$ W/cm^2 at the total internal reflection (TIR) interface. A cooled 2D-charged coupled device (CCD) detector (Cascade-512B; Roper Scientific) was used to image the extremely weak light intensity. Typically, we acquired 300 images sequentially with 100-ms exposures for each. The pixel size (ca. 16 × 16 μm^2) and density (512 × 512 pixels) are both important for obtaining sufficient spatial resolution and imaging area. A combination of super-resolution protocols further increases the resolution [7]. It is also important to discriminate signals from background noise efficiently. Further details were reported previously [6, 10].

3. Results and discussion

First, the sample preparation is essential for the experiments. Here, we simply give the yield of CD-CPN/Cy5 conjugate formations for this purpose. Figure 2 shows a typical single-molecule TIRF microscopy image of QD-CPN conjugates immobilized on the surface of silica glass and sealed with phosphate-buffered saline (PBS). The conjugate formation yield was determined from the ratio of the number of overlaid spots (c) within the observed frame to that of single QD spots (a); the typical yield was ca. 35%, although it sometimes exceeded 70%, which was much better than reported in studies of PFD, in which it was 5% at most [7, 9].

The coincident QD (a) and CPN/Cy5 spots (b) were discriminated using custom-made macro-functions prepared with Igor Pro (ver. 6), which includes the so-called super-resolution protocol. Note that these coincident spots are still simply candidate true conjugates. Next, we inspected the temporal traces of the modulation features of the candidates, followed by noise reduction and the fitting analyses described below. Here, we present two examples as possible detection of the CPN dynamics.

Figure 3 shows the temporal profiles of the rotating analyzer-modulated spot intensities of a QD conjugated with Cy5-labeled CPNs. These were obtained from different samples. In both samples, the CPN concentration was ~1 nM and that of ATP was ~1 mM. The modulation periods, *i.e.*, half of the rotation period, in (a) and (b) were T = 1.37 and 1.38 s, respectively, although the evolution time in (b) was as long as 60 s without any distinct blinking or photodegradation.

In Figs. 3a1 and 3b1, the red lines are the observed spot intensities deduced from the CCD pixels at the specific spots for 100-ms time bins. The blue lines are the fitting results of maximum-likelihood estimator (MLE) analysis [6]. MLE analysis is more suitable than the least-square method if the measured photon density is extremely low. Briefly, in MLE analysis, we can define the likelihood function L as a function of the distributions of the statistic events within the each observed period T. L should be maximized with respect to the fitting parameters M_i (= a_i/b_i), b_i and ϕ_i through the fitting function $y(t_i) = b_i [M_i \cos\{(2\pi\, t_i/T) + \phi_i\} + 1]$. Here, a_i is the modulation amplitude, b_i is the average intensity in each period T, M_i is the modulation depth, which is related to the polar angle θ_i by $\cos^2\theta_i = (1 - M_i)/(1 + M_i)$, $\Delta t = t_{j(i)} - t_{j(i)-1}$ is the time bin of each exposure and is kept constant, *i.e.*, 100 ms, in this experiment. ϕ_i is an initial phase. The subscript $j(i)$ is a time-bin number and runs from 1 to k during time T, where k is the maximum integer $\leq T/\Delta t$, and is ordinarily on the order of 10.

Sequential determination of the best-fit values in every period of T eventually gives rise to the time trajectory of the spatial orientation ($\theta(t)$, $\phi(t)$) of the c-axis direction of the probe QD with a time resolution of T. Figures 3a2 and 3b2 show the temporal evolution profiles of the respective best-fit parameters. Here, we concentrate on whether these time features reflect actual protein motions or artifacts.

At first glance, the data and the fitted curves in Figs. 3a1 and 3b1 suggest that MLE analyses works sufficiently well. Such cases are still rather rare. That is, the temporal resolution or signal-to-noise (S/N) ratio of the observations seems insufficiently optimized to make definitive conclusions. In fact, the number of examples is currently inadequate, so we describe our working hypothesis first, and then compare it with the observed features. The obtained profiles of the fitting parameters shown in Figs. 3a2 and 3b2 still suggest some possibilities.

For this protein, it is important to understand the relationship between ATP binding and hydrolysis events and lid-closure in CPNs [11, 12]. We postulated a two-step model for the conformational changes. As suggested previously [11, 13], this structural transition consisting of ATP binding and the hydrolysis steps should be resolved. ATP binding can already generate

the initial step in lid-closure; it causes apical domain rotation of ca. 45° on the order of 1 s or less, with a slight decrease in cavity volume. Full closure is associated with ATP hydrolysis and manifests as an overall twisting motion of the entire body over a longer time scale. These slower dynamics are another attractive point for prototype studies, especially in single-molecule imaging [14].

We define a successive 3D orientation change $\angle(i-1, i)$ for convenience (red graphs); the angular change of the directional unit vector of the *c*-axis from the $(i-1)^{\text{th}}$ to the i^{th} period. The changes below ca. 10° should be excluded as noise in this experiment. We should also exclude the initial and final parts of the graph as containing artifacts. Therefore, conspicuous changes exceeding ca. 20° are selected as possible candidates indicative of protein-related motions and are numbered from 1 to 4 and 1 to 6, respectively.

The ATP concentration is sufficient for several ATP binding events to occur on our experimental time scale, while other conditions, such as the coexistence of Mg^{2+}+K^{+} for promoting ATP hydrolysis, are not controlled. If we can assume that the CPN conjugates are immobilized in an upright position on the substrate surface, the θ and ϕ components of the QD *c*-axis motion would more directly reflect the θ and ϕ motion of the lid-composing HP. Although this hypothesis was not confirmed for our samples, reported transmission electron microscopy (TEM) observations support this morphology [2]. According to this assumption, the ATP binding will first be revealed by a detectable θ change of around 45°, with an almost negligible ϕ change on the order of 1 s or less. If ATP hydrolysis then occurs, a larger ϕ change will follow on a longer time scale. Such trends seem to appear in the observed features of the θ and ϕ components. Events #2 and #5 in Fig. 32b are the most promising. Half of the observed events should be returns from the partly or fully closed state to the initial open state. In this analysis, although it is in principle possible to classify them by clockwise or counterclockwise movement, we do not distinguish them here mainly due to the insufficient time resolution and save this for future studies, including the effects of the linker itself [15].

Finally, we show two additional features in Fig. 4. The emission intensity of QD conjugated to CPN seems to be reduced by a factor of 2 – 3 compared to free QDs. This may be due to energy transfer to the Cy5s. Interestingly, the conjugated QDs also show reduced blinking. The origin of this feature is not clear, but it appears to be general. Although empirical, these two features seem to support conjugate selection.

In summary, although our results are far from conclusive, our initial trials to capture the dynamics of CPNs at the single-molecule level can be interpreted positively. Further improvements are currently in progress, involving not only ATP binding/hydrolysis timing control, such as stopped-flow type and photo-release injection of ATP, but also an increased S/N ratio data analysis with a higher time resolution. With regard to the latter, a 3 – 5-fold improvement is critical and should provide definitive information in the near future.

Acknowledgements

This work was partly supported by grant-in aid No. 23651105 from the Ministry of Education, Science, Sports, and Culture of Japan.

References:

[1] B. O. Dabbousi, J. Rodriguez-Viejo, F. V. Mikulec, J. R. Heine, H. Mattoussi, R. Ober, K. F. Jensen, M. G. Bawendi, *J. Phys. Chem. B*, **101** (1997) 9463-9475.

[2] J. M. Klostrance, W. C. W. Chan, *Adv. Mater.*, **18** (2006) 1953-1964; I. L. Medintz, H. T. Uyeda, E. R. Goldman, H. Mattoussi, *Nat. Mater.*, **4** (2005) 435-446.

[3] A. L. Efros, M. Rosen, M. Kuno, M. Nirmal, D. J. Norris, M. G. Bawendi, *Phys. Rev. B*, **54** (1996) 4843-4856.

[4] J. Sepiol, J. Jasny, J. Keller, U. P. Wild, *Chem. Phys. Lett.*, **273** (1997) 444-448.

[5] I. Chung, K. T. Shimizu, M. G. Bawendi, *Proc. Natl. Acad. Sci. USA*, **100** (2003) 405-408.

[6] T. Tani, H. Sakai, E. Usukura, T. Suzuki, M. Oda, *Physics Procedia* **3** (2010) 1607-1613.

[7] H. Horiuchi, E. Usukura, A. Ohtaki, T. Zako, M. Oda, M. Yohda, T. Tani, *J. Lumin.*, **127** (2007) 192-197.

[8] T. Tani, K. Mashimo, T. Suzuki, H. Horiuchi, M. Oda, *J. Lumin.*, **128** (2008) 757-760.

[9] T. Tani, H. Horiuchi, M. Oda, E. Usukura, H. Sakai, A. Ohtaki, M. Yohda, *Phys. Status Solidi* **C6** (2009) 912-915.

[10] T. Tani, M. Oda, H. Sakai, D. Araki, Y. Itoh, A. Ohtaki, M. Yohda, *J. Lumin.*, **131** (2011) 519-522.

[11] H. Sekiguchi, A. Nakagawa, K. Moriya, K. Makabe, K. Ichiyanagi, S. Nozawa, T. Sato, S. Adach, K. Kuwajima, M. Yohda, Y. C. Sasaki, *PLOS one*, **8**(5) (2013) e64176.

[12] J. Zhang, B. Ma, F. DiMaio, N. R. Douglas, L. A. Joachimiak, D. Baker, J. Frydman, M. Levitt, W. Chiu, *Structure*, **19** (2011) 633-639.

[13] A. Nakagawa, K. Moriya, M. Arita, Y. Yamamoto, K. Kitamura, N. Ishiguro, T. Kanzaki, T. Oka, K. Makabe, K. Kuwajima, M. Yohda, to appear in *J. Mol. Biol*.

[14] K. R. Willison, *Structure*, **19** (2011) 754-755.

[15] P. C. Nelson, C. Zuria, D. Brogioli, J. F. Beausang, L. Finzi, D. Dunlap, *J. Phys. Chem. B*, **110** (2006) 17260-17267.

Figure Captions

Fig.1 Schematic representation of the QD-CPN/Cy5 conjugate structure and the preparation protocol. The CPN subunit is segmented into apical (green), intermediate (blue), and equatorial (red) domains. The QD is linked to the apical domain at the top of the helical protrusion. We performed all chemical reactions at room temperature in buffer solutions using specific starting components, such as SMCC linker and Cy5 molecular probe.

Fig.2 Typical examples of total internal reflection fluorescence (TIRF) microscopy imaging of single-molecule QD-CPN conjugates immobilized on silica glass sealed with PBS; the spots from (a) single QDs obtained with irradiation at λ_{ex} = 532 nm and (b) single CPN-Cy5's with λ_{ex} = 633 nm in the same area of the sample. (c) Superposition of (a) and (b). The numbered circles in (c) indicate those judged to coincide with each other using our custom protocols. These are candidates for actual conjugate systems (see text). Spots i1 and i2 are judged to be isolated ODs and are referred to in Fig. 4. Each image is the summation of 300 sequentially acquired CCD images with 100-ms exposures to facilitate visibility and measure immobilization.

Fig.3 Two typical temporal profiles of the rotating analyzer-modulated spot intensities of QDs conjugated with Cy5-labeled CPN (a1 and b1) and the results of MLE analyses (a2 and b2, respectively). In a1 and b1, the red lines are the experimental data and the blue lines are the MLE fitting results. The modulation depth M, polar angle θ, and initial phase of longitudinal angle ϕ in a2 and b2 are the fitting parameters used in the MLE analysis. (θ, ϕ) gives a directional coordinate of the c-axis orientation of the single CPN-attached QD. This eventually gives rise to the spatiotemporal evolution of the movement of the helical protrusion with a time resolution of T. $\angle(i-1, i)$ defines the 3D orientation change of the orientation unit vector in the i^{th} period since the $(i-1)^{th}$ period. For the numbered portions, see the details in the text.

Fig.4 Typical temporal evolution profiles of the spot intensities of (a and b) single isolated QDs (#i1 and #i2 in Fig. 2c) and (c and d) those of the QDs conjugated with CPNs (spots #1 and #7). The rotating analyzer was removed for these observations.

Fig.1

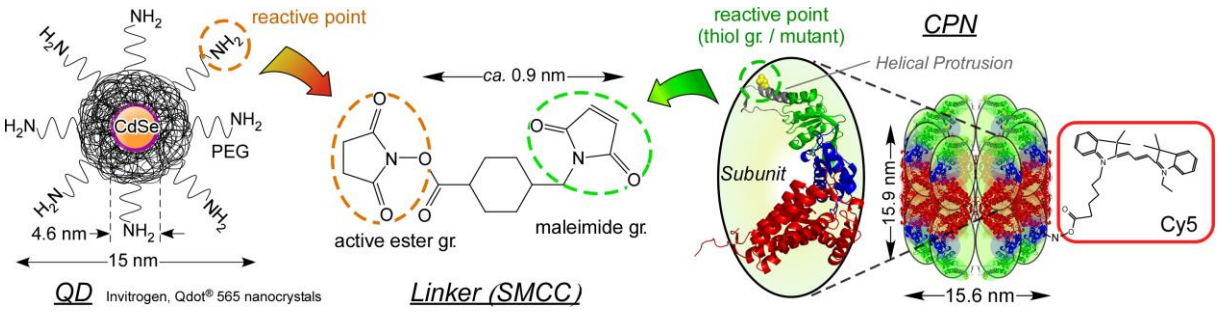
reactive point
ca. 0.9 nm
reactive point
(thiol gr. / mutant)
CPN
Helical Protrusion
NH2
H2N
CdSe
PEG
4.6 nm
15 nm
active ester gr.
maleimide gr.
Subunit
15.9 nm
15.6 nm
Cy5
QD
Invitrogen, Qdot® 565 nanocrystals
Linker (SMCC)

Fig.2

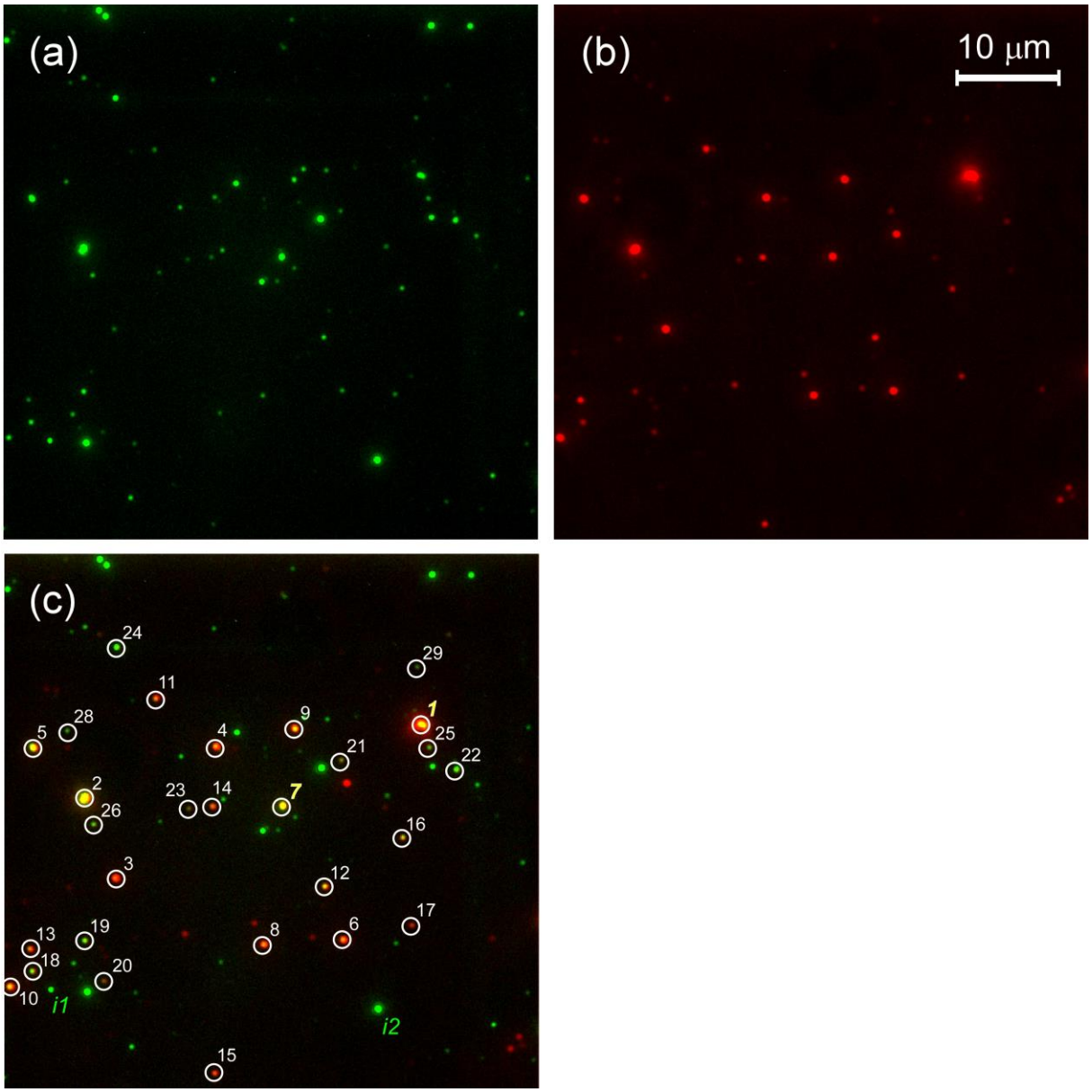
(a)
(b)
10 μm
(c)
24
11
28
5
4
9
1
29
25
21
22
2
26
23
14
7
16
3
12
17
13
19
18
20
8
6
10
i1
i2
15

Fig.3

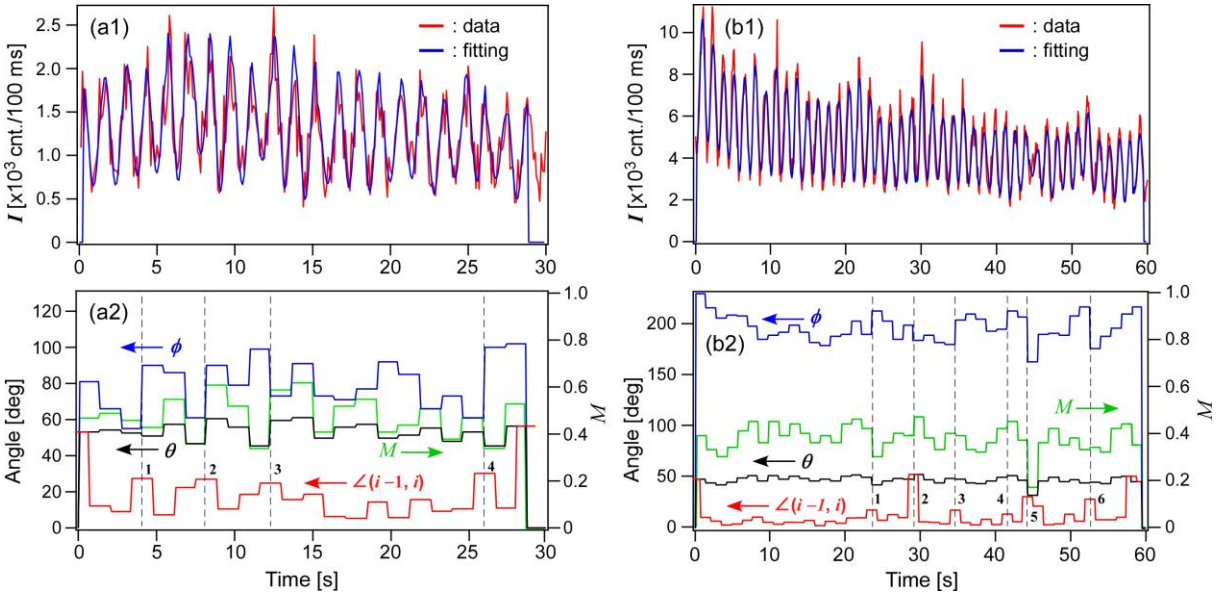
(a1)
: data
: fitting
I [x10^3 cnt./100 ms]
(a2)
ϕ
θ
M
∠(i −1, i)
Angle [deg]
Time [s]
(b1)
: data
: fitting
I [x10^3 cnt./100 ms]
(b2)
ϕ
θ
M
∠(i −1, i)
Angle [deg]
Time [s]

Fig.4